NANO LETTERS

pubs.acs.org/NanoLett Letter

Voltage-Induced Single-Molecule Junction Planarization

Yaping Zang,[⊥] E-Dean Fung,[⊥] Tianren Fu, Suman Ray, Marc H. Garner, Anders Borges, Michael L. Steigerwald, Satish Patil, Gemma Solomon,* and Latha Venkataraman*

Cite This: *Nano Lett.* 2021, 21, 673−679 Read Online

ACCESS | Metrics & More | Article Recommendations | Supporting Information

ABSTRACT: Probing structural changes of a molecule induced by charge transfer is important for understanding the physicochemical properties of molecules and developing new electronic devices. Here, we interrogate the structural changes of a single diketopyrrolopyrrole (DPP) molecule induced by charge transport at a high bias using scanning tunneling microscope break junction (STM-BJ) techniques. Specifically, we demonstrate that application of a high bias increases the average nonresonant conductance of single Au−DPP−Au junctions. We infer from the increased conductance that resonant charge transport induces planarization of the molecular backbone. We further show that this conformational planarization is assisted by thermally activated junction reorganization. The planarization only occurs under specific electronic conditions, which we rationalize by ab initio calculations. These results emphasize the need for a comprehensive view of single-molecule junctions which includes both the electronic properties and structure of the molecules and the electrodes when designing electrically driven single-molecule motors.

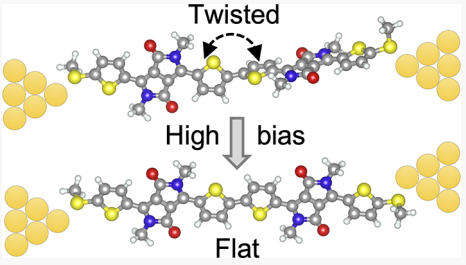

KEYWORDS: *Molecular planarization, Resonant Transport, Single-Molecule Conductance, Diketopyrrolopyrrole*

Changes in the molecular electron density distribution, either by optical excitation or redox events, often result in structural reorganization. The ability to detect the structural changes of molecules in different electronic configurations is critical for the interpretation of molecular physicochemical properties and the development of functional electronic devices. The relation between electronic structure and geometric conformation has been studied in single molecules via optical characterization[1,2] and scanning tunneling microscopy (STM).[3−7] However, the study of electrically induced conformational change in single-molecule devices where the molecule is well-coupled to the electrodes is more limited.[8−11] Here, we use the STM-break junction technique (STM-BJ)[12,13] to measure the conductance of diketopyrrolopyrrole-based single-molecule junctions and show that the molecular junction structure depends on whether transport is in the off-resonant tunneling regime or in the resonant transport regime. Specifically, we show that in the resonant regime, the molecular backbone planarizes due to a change in its electronic character. Distinctions between the off-resonant and resonant transport are achieved by controlling the bias applied across the junction; thus, we are able to drive conformational change electronically. These findings advance our understanding of the relationship between electronic and nuclear degrees of freedom in electrically driven single-molecule motors.

In this study, we present charge transport measurements of a diketopyrrolopyrrole derivative, DPP2.[14−17] This molecule is synthesized according to previously reported procedures.[14] As shown in Figure 1a, DPP2 contains two consecutive donor−acceptor−donor (D-A-D) units composed of an electron-deficient DPP core flanked by two electron-rich thiophene units. The unique D-A-D structure enables efficient intramolecular electron delocalization and a small optical gap.[17−19] Two terminal thioether groups are introduced as linkers to bind to gold electrodes to form stable single Au−molecule−Au junctions.

To measure the conductance of these junctions, we utilize the STM-BJ technique using a custom instrument described in Supporting Information (SI).[13] In brief, we repeatedly drive a Au STM tip in and out of contact with a Au substrate in a dilute solution (0.1−1 mM) of DPP2 in tetradecane (TD) at room temperature. After breaking the Au−Au point contact, a DPP2 molecule can bind to the electrodes and form a single Au−molecule−Au junction. Figure 1b shows sample conductance−displacement traces where a conductance plateau at the quantum of conductance G_0 ($2e^2/h$) signifies the formation of Au−Au point contact. After breaking the Au−Au point contact, molecular conductance plateaus are visible (Figure 1b), evidencing the formation of single Au−DPP2−Au junctions. At a low tip bias of 0.1 V, a conductance plateau at $\sim 3 \times 10^{-5}$ G_0 appears, extending ∼1.5 nm (red). Increasing the tip bias to 1.1

Received: October 25, 2020
Revised: December 5, 2020
Published: December 18, 2020

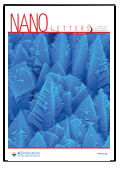

https://dx.doi.org/10.1021/acs.nanolett.0c04260
Nano Lett. 2021, 21, 673−679

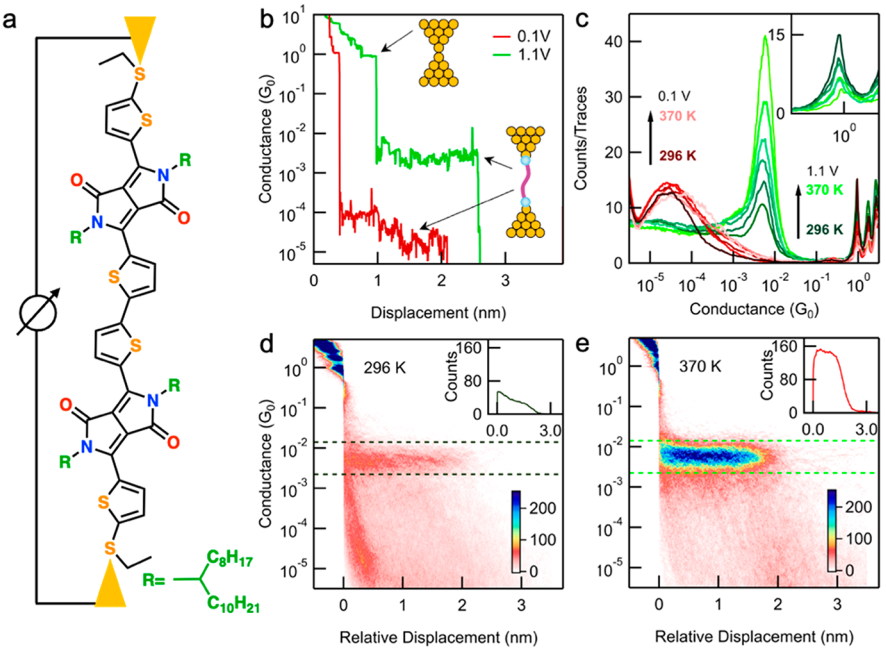

Figure 1. (a) Illustration of a DPP2 molecule held between two Au electrodes during the STM-BJ measurement. (b) Sample conductance−displacement traces for DPP2 measured in TD at 0.1 V (red) and 1.1 V (green). (c) Logarithmically binned 1D histograms for DPP2 at different temperatures measured at both low and high biases. Bin size is 100 bins/decade. Inset shows high bias experiment at different temperatures near 1 G_0. (d,e) Two-dimensional conductance−displacement histograms for DPP2 measured in TD at 1.1 V at (d) 296 K and (e) 370 K. The counts are normalized to the number of traces collected, and the color scales are set equal for direct comparison. The inset shows a line profile which sums the normalized counts within the dashed lines for each relative displacement bin.

V results in a plateau of similar extension at a much higher conductance (green).

In order to obtain statistically representative conductance data, we repeat the measurement thousands of times at each tip bias and compile these traces into logarithmically binned one-dimensional conductance histograms without any data selection. In these histograms, peaks close to integer multiples of G_0 indicate formation of Au point contacts (Figure 1c). The data collected at 0.1 V yields a molecular conductance peak around $\sim 3 \times 10^{-5}$ G_0 (red), whereas the high bias measurement results in a peak centered at a higher conductance of $\sim 5 \times 10^{-3}$ G_0 (green). We have demonstrated previously that the two peaks correspond to off- and on-resonant charge transport, respectively.[14]

Next, we repeat the conductance measurements at different temperatures. We see a stark temperature dependence in the conductance histograms measured at a high bias resonant regime, whereas there is almost no change at a low bias. As can be seen in Figure 1c, the height of the high-bias conductance peak increases by almost a factor of 4 between 296 and 370 K, whereas that at low-bias does not change. We note that the conductance peak positions do not vary with temperature, indicating that this is indeed a coherent transport mechanism and not a hopping mechanism.[14,15] This temperature-dependent increase is in contrast to what is observed for the 1 G_0 peak (shown inset), where the height actually decreases with increasing temperature due to the increased mobility of Au surface atoms.[20,21]

The interpretation of the increase in peak height becomes clearer upon analysis of the 2D conductance−displacement histograms. These histograms are constructed by aligning the individual traces to the location where the junction transitions from a Au−Au point contact to a single-molecule junction.[22] The 2D histograms of resonant tunneling junctions are shown in Figure 1d,e for two different temperatures (see SI Figure S1 for 2D histogram of the low-bias data). At room temperature, we observe that many junctions rupture, as evidenced by the decrease in intensity of the plateau at $\sim 5 \times 10^{-3}$ G_0 with increasing relative displacement. By contrast, the experiment performed at elevated temperature shows a comparatively clean conductance plateau. These are more clearly seen in the line profile for each temperature, shown as an inset. This indicates that the junction stability is increased by increasing temperature.

Single-molecule junctions are known to be unstable in the resonant tunneling regime due to the increased coupling to the nuclear degrees of freedom.[23−26] This is consistent with the observed junction instability at high bias at room temperature. However, the increase of stability at high bias with increasing temperature strongly suggests that the source of junction rupture is due, in large part, to a bias-induced conformational change which can be more easily accommodated at elevated temperatures with an improved mobility of the Au atoms. At low temperatures, the electrodes are more rigid, and a large molecular conformational change is likely to result in junction rupture. As the temperature increases, the Au electrodes are more flexible and can permit modest displacements in the molecule's terminal linker groups.

To both confirm and better characterize the nature of the conformational change, we perform a modified break-junction measurement where the junction is held for 250 ms, during which time the bias voltage is toggled between a low and high state. An example conductance trace measured in TD is shown in Figure 2a. We see in the initial 50 ms of holding the junction at a low bias of 0.5 V (off-resonant regime) that the conductance is low. Once the junction bias is increased to 1.1 V (resonant regime), the conductance increases by more than 2 orders of magnitude and remains high during the 150 ms hold, consistent with what is observed in Figure 1c. This increase in conductance

https://dx.doi.org/10.1021/acs.nanolett.0c04260
Nano Lett. 2021, 21, 673−679

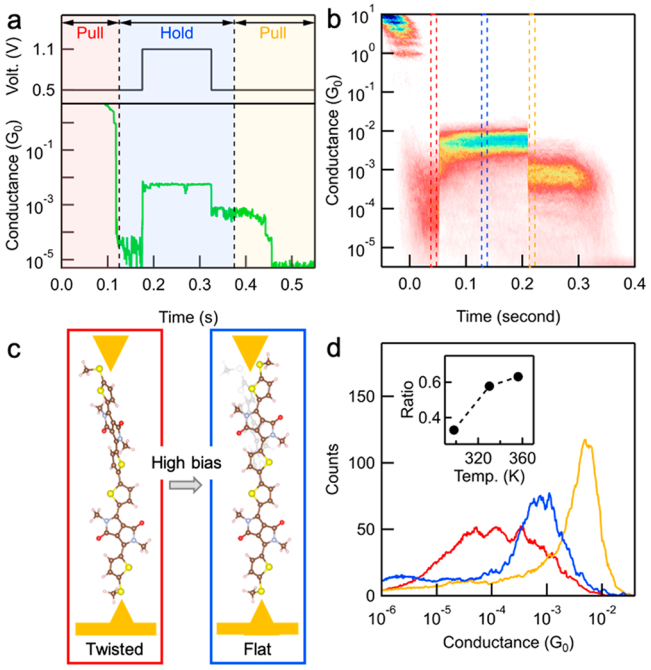

Figure 2. (a) Applied bias (black) and a sample conductance trace (green) acquired during a modified STM-BJ measurement at 330 K where the junction is held for 0.25 s, indicated by the blue shaded region. (b) Two-dimensional conductance histogram compiled from ∼1400 conductance traces with a molecular conducting feature at the start of the hold segment, selected from 2000 measured traces measured at 330 K. (c) Illustration of a change in molecular junction geometry involving a relocation of the attachment point to the STM tip as a result of planarization. (d) Conductance line profiles determined from the 2D histogram shown in (b). Inset: The fraction of junctions that retains planar structure when the bias is decreased as a function of temperature. This fraction is determined from the ratio of the number of traces that increase their conductance after the high-bias is applied relative to those that do not as detailed in the SI.

is expected at resonance and does not evidence a change of conformation as a simple planarization is unlikely to result in a factor of 2 increase in conductance.[12] However, when the bias is switched back to 0.5 V, although the conductance drops it is still higher than the conductance in the initial low-bias segment. This clearly indicates that the high-bias induced resonant transport changes the junction structure resulting in an increased off-resonant conductance.

Figure 2b shows the 2D conductance-time histogram compiled from ∼1400 traces that sustain a molecular junction during the initial 50 ms low bias segment. The three regions, before (red), during (blue), and after (yellow) the high bias hold, show distinct conductance distributions as seen from the conductance profiles in Figure 2d. During the initial low-bias segment, the conductance distribution extends from 10^{-5} to 10^{-3} G_0. This large variance in conductance is frequently observed in break-junction measurements of long molecular wires that have internal rotational degrees of freedom and is attributed to the large variations of junction configuration during junction elongation and from junction to junction.[12,27] By contrast, the distribution of conductance when the high bias is applied is very narrow. Upon reverting to a low bias, the conductance distribution is both narrower and higher than that of the initial low-bias segment, demonstrating the effect of the high-bias on restructuring the junction to enable a higher conductance at low-bias is highly reproducible.

Because the DPP unit is a rigid planar π-system due to a strong donor−acceptor interaction, the conformational degree of freedom that likely controls the junction conductance is the central dihedral angle connecting the two DPP units.[18,28] In the experiments, we expect that the central dihedral varies from junction to junction. When the bias is increased to enable resonant transport, the molecule planarizes. Upon reverting to a lower bias, the molecule retains a planar or near planar structure which results in an increased average conductance.[12] The remaining distribution seen at low bias is likely due to other factors that control the conductance such as the terminal Au−S−C−C dihedrals and the bond orientation. Our results strongly suggest, therefore, that we can drive molecular planarization electrically.

For molecules without axial symmetry, as is the case for thiophene-based oligomers, different rotational conformers place significant constraints on the position of the electrodes. Planarizing the molecule by rotating the central dihedral requires reorganization of the molecule−electrode bond that can have a large energy cost, as illustrated in Figure 2c. By contrast, oligophenylenes, which have an axial symmetry, can planarize without changes to the orientation of the terminal ligand−electrode bonds.[27] Measurements at higher temperatures facilitate the reorganization in DPP2 junctions likely due to the increased mobility of Au atoms. Once the molecule planarizes at a high bias without breaking contact to the electrodes, in the absence of any driving force toward a more twisted structure, the junction will remain planar. In other words, the planar conformation is locked in the junction, and the molecule does not revert back to a twisted geometry when the bias is decreased. To quantify the effect of temperature on facilitating this planarization, we repeat the measurement shown in Figure 2a at different temperatures (see SI Figure S2). Results at room temperature and at 356 K are similar. However, the fraction of junctions that evidence a planar molecule increases with temperature, reaching close to 65% at 356 K (inset, Figure 2d).

Having argued that resonant transport induced planarization best explains our experimental results, we now investigate the mechanism by which resonant charge transport induces planarization. Planarization upon redox events and optical excitation is often attributed to the increase in quinoidal character of the molecule.[29−31] We suggest that the same is true during resonant transport. The transport electrons have longer lifetimes on the molecule in the resonant tunneling regime than in the off-resonant tunneling regime and can modify the electron distribution on the molecule.[32] We hypothesize that resonant charge transport increases the quinoidal character of the molecular electronic states, which drives planarization, similar to what has been observed before.[8]

The possible mechanisms for planarization is narrowed by repeating the experiments in a different nonpolar solvent, 1,2,4-trichlorobenzene (TCB), as shown in SI Figure S3. Surprisingly, although we still observe resonant transport, we do not observe planarization in experiments performed either in TCB or Nonanol (see SI Figure S4). To understand the difference between junctions in TCB compared with those in TD, we obtain the average current−voltage (I−V) characteristics of DPP2 in TD and TCB by repeating break-junction measurements thousands of times at a range of applied voltages (see SI Figure S5). We see that the current first increases with increasing bias voltage and then saturates (Figure 3a). This indicates a transition from off-resonant tunneling transport to resonant

https://dx.doi.org/10.1021/acs.nanolett.0c04260
Nano Lett. 2021, 21, 673−679

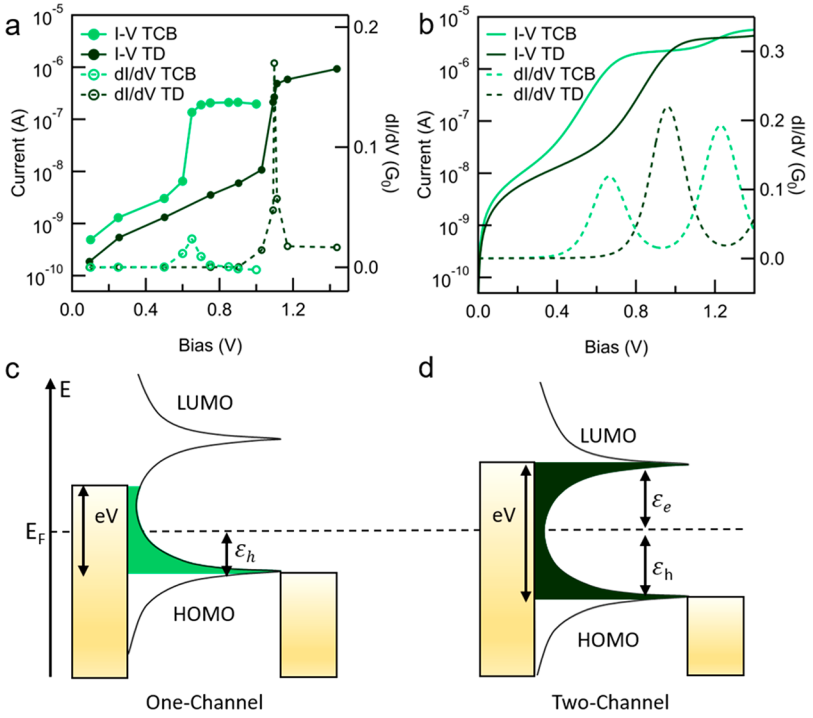

Figure 3. (a) Current−voltage (I−V) and differential conductance (dI/dV) for DPP2 in TCB (light green) and TD (dark green). (b) Calculated I−V and dI/dV from transmission functions shown in SI Figure S7. The Fermi energy is shifted by 0.14 eV to model midgap transport in TD. Energy diagram illustrating (c) single-channel and (d) two-channel transport. Note that the molecule has a net charge in (c), whereas it is neutral in (d).

transport at high bias when the dominant transport orbital falls within the bias window.[33−36] The numerically obtained differential conductance (dI/dV) peak indicates the bias at which we achieve resonance. Because these measurements are performed in nonpolar solvent where the junctions are considered to be symmetric, the current measured across a molecular junction at an applied voltage V is approximately the integral of the transmission function over the energy range of ±eV/2.[37] As shown in Figure 3a, a dI/dV peak occurs at 1.1 V when DPP2 is measured in TD, which is in contrast to the peak at 0.65 V for TCB measurements. This indicates that the resonance is ∼0.55 eV relative to E_F in TD compared with ∼0.325 eV in TCB. The difference in energy level alignment is attributed to a static solvent gating effect.[38,39] Through thermopower measurements (Figure S6), we identify that the HOMO is the resonance predominately contributing transport in these junctions. The smaller thermopower obtained in TD suggests that HOMO aligns further away from E_F compared to that in TCB (Figure 3c,d), which is in agreement with the dI/dV results. Importantly, we note that the current measured beyond resonance is higher in TD than in TCB. Such an increase suggests that an additional resonance enters the bias window in TD. We infer that in TD there are two orbitals (HOMO and LUMO) contributing to resonant transport as E_F lies closer to the middle of the HOMO−LUMO gap (Figure 3d). As illustrated in the schematic in Figure 1c, this results in a simultaneous transfer of both electrons and holes across the molecular junction.

We reproduce the charge transport characteristics by calculating I−V and dI/dV curves (Figure 3a,b) using the Landauer formula. We use a transmission function obtained via DFT for a DPP2 junction and assume that the bias window opens symmetrically about E_F (SI Figure S7).[40,41] We use the DFT-based HOMO and LUMO positions relative to E_F to model transport in TCB but horizontally shift the transmission function by 0.14 eV to model a midgap alignment of DPP2 in TD as shown in Figure 3d. The calculated I−V and dI/dV curves are in qualitative agreement with the experimental results, although the positions and magnitudes of the peaks in differential conductance are not accurately captured due to the errors inherent to DFT.[42] The theoretical dI/dV for TCB shows two peaks because the HOMO resonance enters the bias window first, followed by the LUMO resonance at a higher bias. However, we are unable to sustain junctions at biases higher than 1 V experimentally in TCB. By contrast, there is only one peak in the dI/dV for TD since both resonances enter the bias window simultaneously. As in the experiment, the theoretical current at low bias is lower in TD than in TCB due to the closer HOMO in the latter, but the saturation current is higher in TD due to the two-orbital resonant transport.

The lack of evidence of planarization for experiments performed in TCB suggests that resonant electron transport through just the HOMO is not sufficient to drive planarization. To investigate this further, we calculate the rotational barrier of DPP2 (without the side chains) as a function of the central dihedral angle using density functional theory (DFT) for the ground, cationic, anionic, and triplet excited states.[43] A higher torsion barrier represents energy required to twist the dihedral. In the resonant regime, planarizing from a twisted conformation provides sufficient energy to reorganize the nanoscale electrode structure. To use a mechanical analogy, the molecule is like a twisted spring, held in a higher energy conformation by the electrodes. Driving electrons resonantly stiffens the spring which drives the molecule to planarize. A higher thermal energy makes the electrodes more accommodating, allowing the reorganization to occur without breaking the junction.

We find that the cationic and anionic states have higher torsion barriers with respect to the ground state and that the

https://dx.doi.org/10.1021/acs.nanolett.0c04260
Nano Lett. 2021, 21, 673−679

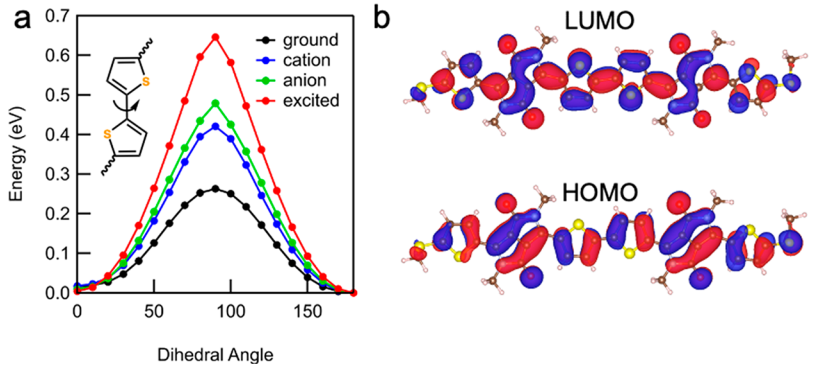

Figure 4. (a) Energy barrier as a function of dihedral angle for the ground, cationic, anionic, and triplet excited states of DPP2. (c) LUMO and HOMO orbital isosurfaces of DPP2 in the ground state, calculated in Jaguar.[44]

excited state has the highest torsion barrier (see Figure 4a). This suggests that although resonant transport through the HOMO should drive planarization of a twisted molecule in a junction, the energy gained may not be sufficient to enable restructuring of the terminal ligand−electrode bonds. Our experiments suggest that resonant transport through both frontier orbitals (see Figure 4b), on the other hand, has a sufficiently large torsion barrier to drive planarization.

Some important qualifications are appropriate. First, the electronic structure in the molecule is affected by the electrodes, and the electric field from the electrodes will polarize the molecule, which can also alter the quinoidal character of the molecule. These effects are not captured in the calculations. Furthermore, resonant transport through both frontier orbitals may be subtly different from an optically excited state due to possibly weak correlation between tunneling electrons and holes. Although advances in theory are required for a more comprehensive understanding of the mechanism for planarization during resonant transport, the agreement between the DFT calculations and our experimental results is promising.[45,46] We also note that planarization was observed in a single molecule junction by Bi et al. without resonant tunneling through both frontier orbitals.[8] We hypothesize that the difference is due to the presence of axial symmetry in that work where planarization does not require significant electrode reorganization, and resonant transport through a single frontier orbital may be sufficient.

In conclusion, we have demonstrated a two-orbital resonant transport mechanism involving both HOMO and LUMO of a single DPP2 molecule which enables the molecule to transition into a bias-induced planar conformation in a junction. In contrast, such a planarization is not observed in the single-orbital resonant tunneling regime. These results open the way to explore the fundamental physics of electronic and conformational reorganization of molecules which otherwise are generally probed by conventional optical techniques.

■ ASSOCIATED CONTENT

Supporting Information

The Supporting Information is available free of charge at https://pubs.acs.org/doi/10.1021/acs.nanolett.0c04260.

STM-BJ measurements methods, DFT calculations, additional experimental data and analysis (PDF)

■ AUTHOR INFORMATION

Corresponding Authors

Gemma Solomon − *Nano-Science Center and Department of Chemistry, University of Copenhagen, Copenhagen Ø DK-2100, Denmark;* orcid.org/0000-0002-2018-1529; Email: gsolomon@chem.ku.dk

Latha Venkataraman − *Department of Applied Physics, Columbia University, New York 10027, United States; Department of Chemistry, Columbia University, New York 10027, United States;* orcid.org/0000-0002-6957-6089; Email: lv2117@columbia.edu

Authors

Yaping Zang − *Department of Applied Physics, Columbia University, New York 10027, United States*

E-Dean Fung − *Department of Applied Physics, Columbia University, New York 10027, United States;* orcid.org/0000-0001-6996-0243

Tianren Fu − *Department of Chemistry, Columbia University, New York 10027, United States;* orcid.org/0000-0002-9008-5241

Suman Ray − *Solid State and Structural Chemistry Unit, Indian Institute of Science, Bangalore 560012, India*

Marc H. Garner − *Nano-Science Center and Department of Chemistry, University of Copenhagen, Copenhagen Ø DK-2100, Denmark;* orcid.org/0000-0002-7270-8353

Anders Borges − *Nano-Science Center and Department of Chemistry, University of Copenhagen, Copenhagen Ø DK-2100, Denmark*

Michael L. Steigerwald − *Department of Chemistry, Columbia University, New York 10027, United States*

Satish Patil − *Solid State and Structural Chemistry Unit, Indian Institute of Science, Bangalore 560012, India;* orcid.org/0000-0003-3884-114X

Complete contact information is available at: https://pubs.acs.org/10.1021/acs.nanolett.0c04260

Author Contributions

⊥These authors contributed equally to this work.

Notes

The authors declare no competing financial interest.

■ ACKNOWLEDGMENTS

Experimental work was supported primarily by the National Science Foundation (DMR-1807580). Suman Ray acknowledges D. S. Kothari postdoctoral fellowship scheme for funding.

Satish Patil thanks Department of Science and Technology, New Delhi, India for a Swarnajayanti fellowship. G.C.S. A.B. and M.H.G. received funding from the Danish Council for Independent Research Natural Sciences and the Carlsberg Foundation.

REFERENCES

(1) Tretiak, S.; Saxena, A.; Martin, R. L.; Bishop, A. R. Conformational dynamics of photoexcited conjugated molecules. *Phys. Rev. Lett.* **2002**, *89*, 097402.
(2) Zhang, Z.; Wu, Y. S.; Tang, K. C.; Chen, C. L.; Ho, J. W.; Su, J.; Tian, H.; Chou, P. T. Excited-State Conformational/Electronic Responses of Saddle-Shaped N,N'-Disubstituted-Dihydrodibenzo-[a,c]phenazines: Wide-Tuning Emission from Red to Deep Blue and White Light Combination. *J. Am. Chem. Soc.* **2015**, *137*, 8509−8520.
(3) Fatayer, S.; Albrecht, F.; Zhang, Y.; Urbonas, D.; Pena, D.; Moll, N.; Gross, L. Molecular structure elucidation with charge-state control. *Science* **2019**, *365*, 142−145.
(4) Borca, B.; et al. Bipolar Conductance Switching of Single Anthradithiophene Molecules. *ACS Nano* **2015**, *9*, 12506−12512.
(5) Palma, C. A.; Joshi, S.; Hoh, T.; Ecija, D.; Barth, J. V.; Auwarter, W. Two-level spatial modulation of vibronic conductance in conjugated oligophenylenes on boron nitride. *Nano Lett.* **2015**, *15*, 2242−2248.
(6) Schaffert, J.; Cottin, M. C.; Sonntag, A.; Karacuban, H.; Bobisch, C. A.; Lorente, N.; Gauyacq, J.-P.; Moller, R. Imaging the dynamics of individually adsorbed molecules. *Nat. Mater.* **2013**, *12*, 223−227.
(7) Stolz, S.; Groning, O.; Prinz, J.; Brune, H.; Widmer, R. Molecular motor crossing the frontier of classical to quantum tunneling motion. *Proc. Natl. Acad. Sci. U. S. A.* **2020**, *117*, 14838−14842.
(8) Bi, H.; Palma, C. A.; Gong, Y.; Hasch, P.; Elbing, M.; Mayor, M.; Reichert, J.; Barth, J. V. Voltage-Driven Conformational Switching with Distinct Raman Signature in a Single-Molecule Junction. *J. Am. Chem. Soc.* **2018**, *140*, 4835−4840.
(9) Brough, B.; Northrop, B. H.; Schmidt, J. J.; Tseng, H. R.; Houk, K. N.; Stoddart, J. F.; Ho, C. M. Evaluation of synthetic linear motor-molecule actuation energetics. *Proc. Natl. Acad. Sci. U. S. A.* **2006**, *103*, 8583−8588.
(10) Hugel, T.; Holland, N. B.; Cattani, A.; Moroder, L.; Seitz, M.; Gaub, H. E. Single-molecule optomechanical cycle. *Science* **2002**, *296*, 1103−1106.
(11) Lussis, P.; Svaldo-Lanero, T.; Bertocco, A.; Fustin, C. A.; Leigh, D. A.; Duwez, A. S. A single synthetic small molecule that generates force against a load. *Nat. Nanotechnol.* **2011**, *6*, 553−557.
(12) Venkataraman, L.; Klare, J. E.; Nuckolls, C.; Hybertsen, M. S.; Steigerwald, M. L. Dependence of single-molecule junction conductance on molecular conformation. *Nature* **2006**, *442*, 904−907.
(13) Xu, B.; Tao, N. J. Measurement of single-molecule resistance by repeated formation of molecular junctions. *Science* **2003**, *301*, 1221−1223.
(14) Zang, Y.; Ray, S.; Fung, E. D.; Borges, A.; Garner, M. H.; Steigerwald, M. L.; Solomon, G. C.; Patil, S.; Venkataraman, L. Resonant Transport in Single Diketopyrrolopyrrole Junctions. *J. Am. Chem. Soc.* **2018**, *140*, 13167−13170.
(15) Skidin, D.; et al. Tuning the conductance of a molecular wire by the interplay of donor and acceptor units. *Nanoscale* **2018**, *10*, 17131−17139.
(16) Li, B.; Yu, H.; Montoto, E. C.; Liu, Y.; Li, S.; Schwieter, K.; Rodríguez-López, J.; Moore, J. S.; Schroeder, C. M. Intrachain Charge Transport through Conjugated Donor−Acceptor Oligomers. *ACS Applied Electronic Materials* **2019**, *1*, 7−12.
(17) Mukhopadhyay, T.; et al. Air-Stable n-channel Diketopyrrolopyrrole-Diketopyrrolopyrrole Oligomers for High Performance Ambipolar Organic Transistors. *ACS Appl. Mater. Interfaces* **2016**, *8*, 25415−25427.
(18) Dhar, J.; Venkatramaiah, N.; Patil, S. Photophysical, electrochemical and solid state properties of diketopyrrolopyrrole based molecular materials: importance of the donor group. *J. Mater. Chem. C* **2014**, *2*, 3457−3466.
(19) Tang, A.; Zhan, C.; Yao, J.; Zhou, E. Design of Diketopyrrolopyrrole (DPP)-Based Small Molecules for Organic-Solar-Cell Applications. *Adv. Mater.* **2017**, *29*, 1600013.
(20) Huang, Z.; Chen, F.; D'Agosta, R.; Bennett, P. A.; Di Ventra, M.; Tao, N. Local ionic and electron heating in single-molecule junctions. *Nat. Nanotechnol.* **2007**, *2*, 698−703.
(21) Tsutsui, M.; Taniguchi, M.; Kawai, T. Local heating in metal-molecule-metal junctions. *Nano Lett.* **2008**, *8*, 3293−3297.
(22) Martin, C. A.; Ding, D.; Sorensen, J. K.; Bjornholm, T.; van Ruitenbeek, J. M.; van der Zant, H. S. Fullerene-based anchoring groups for molecular electronics. *J. Am. Chem. Soc.* **2008**, *130*, 13198−13199.
(23) Fung, E. D.; et al. Breaking Down Resonance: Nonlinear Transport and the Breakdown of Coherent Tunneling Models in Single Molecule Junctions. *Nano Lett.* **2019**, *19*, 2555−2561.
(24) Koch, J.; Semmelhack, M.; von Oppen, F.; Nitzan, A. Current-induced nonequilibrium vibrations in single-molecule devices. *Phys. Rev. B: Condens. Matter Mater. Phys.* **2006**, *73*, 155306.
(25) Li, H.; Su, T. A.; Zhang, V.; Steigerwald, M. L.; Nuckolls, C.; Venkataraman, L. Electric field breakdown in single molecule junctions. *J. Am. Chem. Soc.* **2015**, *137*, 5028−5033.
(26) Stipe, B. C.; Rezaei, M. A.; Ho, W.; Gao, S.; Persson, M.; Lundqvist, B. I. Single-Molecule Dissociation by Tunneling Electrons. *Phys. Rev. Lett.* **1997**, *78*, 4410−4413.
(27) Dell, E. J.; Capozzi, B.; DuBay, K. H.; Berkelbach, T. C.; Moreno, J. R.; Reichman, D. R.; Venkataraman, L.; Campos, L. M. Impact of molecular symmetry on single-molecule conductance. *J. Am. Chem. Soc.* **2013**, *135*, 11724−11727.
(28) Jackson, N. E.; Savoie, B. M.; Kohlstedt, K. L.; Olvera de la Cruz, M.; Schatz, G. C.; Chen, L. X.; Ratner, M. A. Controlling conformations of conjugated polymers and small molecules: the role of nonbonding interactions. *J. Am. Chem. Soc.* **2013**, *135*, 10475−10483.
(29) Burrezo, P. M.; Zafra, J. L.; Lopez Navarrete, J. T.; Casado, J. Quinoidal/Aromatic Transformations in pi-Conjugated Oligomers: Vibrational Raman studies on the Limits of Rupture for pi-Bonds. *Angew. Chem., Int. Ed.* **2017**, *56*, 2250−2259.
(30) Irle, S.; Lischka, H. Combined ab initio and density functional study on polaron to bipolaron transitions in oligophenyls and oligothiophenes. *J. Chem. Phys.* **1997**, *107*, 3021−3031.
(31) Zojer, E.; Cornil, J.; Leising, G.; Brédas, J. L. Theoretical investigation of the geometric and optical properties of neutral and charged oligophenylenes. *Phys. Rev. B: Condens. Matter Mater. Phys.* **1999**, *59*, 7957−7968.
(32) Galperin, M.; Ratner, M. A.; Nitzan, A. Molecular transport junctions: vibrational effects. *J. Phys.: Condens. Matter* **2007**, *19*, 103201.
(33) Brooke, C.; Vezzoli, A.; Higgins, S. J.; Zotti, L. A.; Palacios, J. J.; Nichols, R. J. Resonant transport and electrostatic effects in single-molecule electrical junctions. *Phys. Rev. B: Condens. Matter Mater. Phys.* **2015**, *91*, 195438.
(34) Kuang, G.; Chen, S. Z.; Wang, W.; Lin, T.; Chen, K.; Shang, X.; Liu, P. N.; Lin, N. Resonant Charge Transport in Conjugated Molecular Wires beyond 10 nm Range. *J. Am. Chem. Soc.* **2016**, *138*, 11140−11143.
(35) Perrin, M. L.; Burzuri, E.; van der Zant, H. S. Single-molecule transistors. *Chem. Soc. Rev.* **2015**, *44*, 902−919.
(36) Thomas, J. O.; Limburg, B.; Sowa, J. K.; Willick, K.; Baugh, J.; Briggs, G. A. D.; Gauger, E. M.; Anderson, H. L.; Mol, J. A. Understanding resonant charge transport through weakly coupled single-molecule junctions. *Nat. Commun.* **2019**, *10*, 4628.
(37) Datta, S. *Electronic Transport in Mesoscopic Systems*; Cambridge University Press: Cambridge, 1995.
(38) Choi, B.; Capozzi, B.; Ahn, S.; Turkiewicz, A.; Lovat, G.; Nuckolls, C.; Steigerwald, M. L.; Venkataraman, L.; Roy, X. Solvent-dependent conductance decay constants in single cluster junctions. *Chem. Sci.* **2016**, *7*, 2701−2705.
(39) Fatemi, V.; Kamenetska, M.; Neaton, J. B.; Venkataraman, L. Environmental control of single-molecule junction transport. *Nano Lett.* **2011**, *11*, 1988−1992.

https://dx.doi.org/10.1021/acs.nanolett.0c04260
Nano Lett. 2021, 21, 673−679

(40) Enkovaara, J.; et al. Electronic structure calculations with GPAW: a real-space implementation of the projector augmented-wave method. *J. Phys.: Condens. Matter* **2010**, *22*, 253202.
(41) Hjorth Larsen, A.; et al. The atomic simulation environment-a Python library for working with atoms. *J. Phys.: Condens. Matter* **2017**, *29*, 273002.
(42) Neaton, J. B.; Hybertsen, M. S.; Louie, S. G. Renormalization of molecular electronic levels at metal-molecule interfaces. *Phys. Rev. Lett.* **2006**, *97*, 216405.
(43) Havu, V.; Blum, V.; Havu, P.; Scheffler, M. Efficient integration for all-electron electronic structure calculation using numeric basis functions. *J. Comput. Phys.* **2009**, *228*, 8367−8379.
(44) Bochevarov, A. D.; et al. Jaguar: A high-performance quantum chemistry software program with strengths in life and materials sciences. *Int. J. Quantum Chem.* **2013**, *113*, 2110−2142.
(45) Pshenichnyuk, I. A.; Čížek, M. Motor effect in electron transport through a molecular junction with torsional vibrations. *Phys. Rev. B: Condens. Matter Mater. Phys.* **2011**, *83*, 165446.
(46) Hartle, R.; Schinabeck, C.; Kulkarni, M.; Gelbwaser-Klimovsky, D.; Thoss, M.; Peskin, U. Cooling by heating in nonequilibrium nanosystems. *Phys. Rev. B: Condens. Matter Mater. Phys.* **2018**, *98*, 081404.

https://dx.doi.org/10.1021/acs.nanolett.0c04260
Nano Lett. 2021, 21, 673−679